Transport coefficients for laminar and turbulent flow through a four-cusp channel

A. S. Dutra, P. R. Souza Mendes, and J. A. R. Parise
Department of Mechanical Engineering, Pontifícia Universidade Católica-RJ Rio de Janeiro, Brazil

A study was performed to determine entrance region and fully developed heat transfer coefficients for laminar and turbulent flow in a four-cusp channel, for a thermal boundary condition of uniform wall temperature. A numerical solution was presented for fully developed laminar flow, and an experimental study was reported for turbulent flow. In the experiments, systematic variations of the Reynolds number were made in the range 5300–30,300. The results show that the heat transfer coefficients for the four-cusp channel are much lower than the coefficients for the circular tube.

Keywords: four-cusp channel; naphthalene sublimation technique; LOCA

Introduction

Numerical simulators of accidents in nuclear reactors may be useful tools while analyzing safety features of nuclear PWR plants. These simulations are only possible when related heat transfer information is available.

With the loss-of-coolant accident (LOCA), there is a short period between the initial blowdown and the quenching of the fuel rods by the emergency core cooling system (ECCS), during which the fuel cladding may be exposed to very high temperatures. This causes an excessive increase in the internal pressure, leading to swelling and even rupture of the fuel cladding. The result is that the reactor becomes partially blocked. This blockage can axially extend to several diameters,[1] forming elongated channels. The heat transfer characteristics of these channels are of crucial importance to the effectiveness of the emergency cooling system.

In investigating the shape of such channels, Turner and Haque[2] suggested that adjacent fuel rods, in the process of "ballooning," could touch each other before reaching rupture. In such conditions, and by observing in Figure 1 the results from multirod burst tests made by Kawasaki et al.,[3] it can be concluded that the four-cusp geometry is representative of a degraded core reactor channel.

A number of papers on four-cusp channel flow can be found in the literature. Gunn and Darling[4] performed experimental measurements of the friction factor for a range of Reynolds numbers from 200 to 100,000, covering laminar, transition and turbulent flow. Gerard and Baines[5] also measured the velocity and boundary shear distributions for conditions limited to laminar flow.

As far as heat transfer is concerned, considerable effort[2,6–8] has been put into the analysis of forced convection in four-cusp channels by the Universities of Manchester (Simon Engineering Laboratories) and Liverpool, in the UK. A series of single-phase steady-state experiments have been performed to investigate forced convection in blocked subchannels. The work has been supported by analytical predictions of wall temperature variations and the effects of secondary flows and wall damping. The effects of partial flow blockage in PWR rod bundle geometries have also been studied by Ihle et al.[9,10] More recently, some numerical studies on the laminar flow and heat transfer were reported by Maliska and Silva[11] and also by Nieckele.[12] In an interesting paper, Duck and Turner[13] imposed a uniform heat flux condition at the fuel-cladding interface, and included a thickness of cladding in the analysis. In this conjugate heat transfer problem, conduction through the cladding was handled with a finlike theory, while the (laminar) flow problem was tackled with finite-difference techniques. A transformed domain was employed in the analysis.

The present article deals mainly with an experimental investigation on the heat transfer characteristics of the turbulent flow in a four-cusp channel with uniform wall temperature. In the experiments, the naphthalene sublimation technique was employed. For completeness, a numerical solution of the laminar flow was also performed, as described in the following section.

The analysis

The calculation domain is depicted in Figure 2. It is clear that, due to symmetry, only one eighth of the channel cross section needs to be considered. The formulation presented here pertains to the case of fully developed constant-property laminar flow through the channel under study.

The momentum and energy equations may be written in the following dimensionless forms:

$$\frac{\partial^2\Omega}{\partial\eta^2}+\frac{1}{\eta^2}\frac{\partial^2\Omega}{\partial\theta^2}+1=0 \tag{1}$$

$$\frac{\partial^2\phi}{\partial\eta^2}+\frac{1}{\eta^2}\frac{\partial^2\phi}{\partial\theta^2}+\lambda\phi\frac{\Omega}{\bar{\Omega}}=0 \tag{2}$$

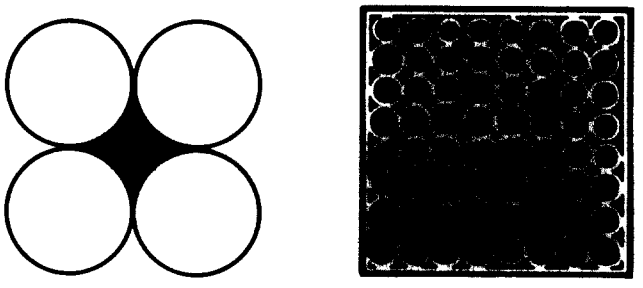

Figure 1 A PWR degraded core[3] and the four-cusp geometry

Address reprint requests to Professor Mendes at the Department of Mechanical Engineering, Pontifícia Universidade Católica-RJ, Rua Marquês de São Vicente 225, Rio de Janeiro, RJ 22453, Brazil.

Received 6 September 1990; accepted 16 November 1990

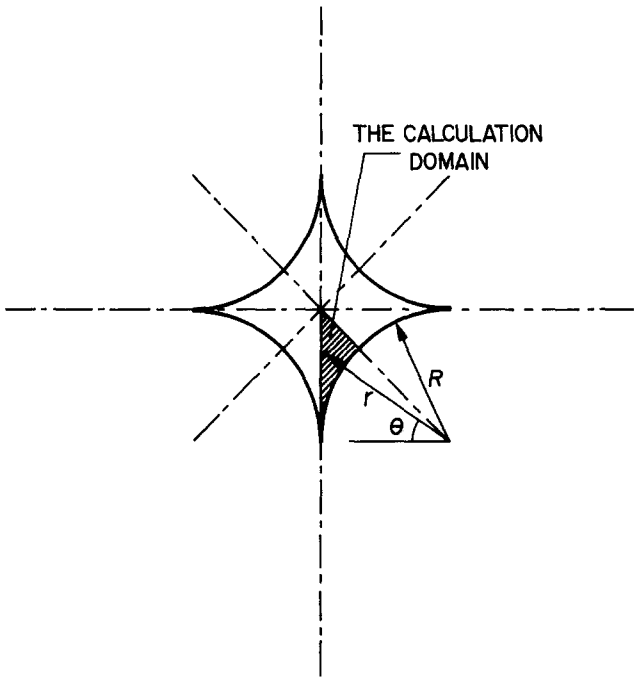

Figure 2 The four-cusp channel with the calculation domain

In Equation 1, the dimensionless velocity Ω is defined as

$$\Omega \equiv \frac{w\mu}{(-dp/dz)D_h^2} \tag{3}$$

where w denotes the axial velocity (in the z direction), p is the pressure, μ is the absolute viscosity, and D_h is the hydraulic diameter. This latter quantity is given by

$$D_h = 2R\frac{4-\pi}{\pi} \tag{4}$$

The quantity η is the dimensionless radial coordinate, defined (see Figure 2) as

$$\eta \equiv \frac{r}{D_h} \tag{5}$$

and θ is the angular coordinate.

In Equation 2, ϕ is the dimensionless temperature, defined as

$$\phi \equiv \frac{T-T_w}{T_b-T_w} \tag{6}$$

where T_w is the channel wall temperature and T_b is the bulk temperature of the flowing fluid.

The constant λ is defined as

$$\lambda = \frac{-d(T_b-T_w)/dZ}{T_b-T_w} \tag{7}$$

Notation

a	A dimensionless constant (Equation 12)
A_w	Area of mass transfer, m^2
c_p	Specific heat at constant pressure, J/kg K
D_h	Hydraulic diameter (Equation 4), m
f	Friction factor, $\equiv 2(-dp/dz)D_h/\rho\bar{w}^2$, dimensionless
h	Heat transfer coefficient, W/m^2 K
$\bar{h}$	Average heat transfer coefficient, W/m^2 K
i	Module identification number, dimensionless
K_i	Per-module mass transfer coefficient, J/kg
k	Thermal conductivity, W/m K
M_i	Net variation in the module mass, kg
$\dot{M}_i$	Per-module mass transfer rate, kg/s
$\dot{m}$	Air flow rate, kg/s
M_n	Molecular weight of naphthalene, kg/kmol
n	Coordinate normal to boundary of domain, m
Nu	Local Nusselt number in the fully developed region, dimensionless
$\overline{\text{Nu}}$	Mean value of Nu, averaged along wall in θ-direction, dimensionless
$\overline{\text{Nu}}_{ct}$	Nusselt number for the fully developed flow in a circular tube, dimensionless
p	Pressure, Pa
p_{nw}	Vapor pressure of naphthalene at wall (Equation 18), Pa
Pe	Péclét number $\equiv$ Re Pr, dimensionless
Pr	Prandtl number (Equation 10), dimensionless
r	Radial coordinate, m
R	Radius of curvature of wall, m
$\mathscr{R}$	Universal gas constant, J/kmol K
Re	Reynolds number (Equation 9), dimensionless
Sc	Schmidt number, dimensionless
Sh	Sherwood number at a given axial location, averaged along wall in θ-direction, dimensionless
Sh_{fd}	Value of Sh in the fully developed region of flow, dimensionless
Sh_i	Per-module average Sherwood number (Equation 21), dimensionless
T	Temperature, K
T_b	Bulk temperature, K
T_w	Wall temperature, K
w	Axial velocity, m/s
$\bar{w}$	Mean value of w in the cross section, m/s
w_{max}	Maximum value of w in the cross section, m/s
Z	Dimensionless axial coordinate (Equation 8)
z	Axial coordinate, m

Greek symbols

$\Delta\rho_{n,i}$	Wall-to-bulk difference in naphthalene vapor density for module i (Equation 17), kg/m^3
η	Dimensionless radial coordinate (Equation 5)
θ	Angular coordinate, rad
λ	A dimensionless constant (Equation 7)
μ	Absolute viscosity, kg/m s
ν	Kinematic viscosity, m^2/s
ρ	Mean air density, kg/m^3
$\rho_{\text{nb},i}$	Bulk density of naphthalene vapor immediately downstream of the ith module (Equation 19), kg/m^3
ρ_{nw}	Naphthalene vapor density at channel wall, kg/m^3
τ	Duration of the experimental run, s
ϕ	Dimensionless temperature (Equation 6)
Ω	Dimensionless axial velocity (Equation 3)
$\bar{\Omega}$	Mean value of Ω in the cross section, dimensionless
Ω_{max}	Maximum value of Ω in the cross section, dimensionless

In the above equation, Z is the dimensionless axial coordinate, given by

$$Z \equiv \frac{z/D_h}{\mathrm{Pe}} \tag{8}$$

The Péclét number Pe is given by the product between the Reynolds number Re and the Prandtl number Pr, i.e., $\mathrm{Pe} \equiv \mathrm{Re}\,\mathrm{Pr}$. Re and Pr are defined, respectively, as

$$\mathrm{Re} \equiv \frac{\rho \bar{w} D_h}{\mu} \tag{9}$$

and

$$\mathrm{Pr} \equiv \frac{\mu c_p}{k} \tag{10}$$

Since λ is not known a priori, a subsidiary equation is needed. For this purpose, the nondimensional counterpart of the definition of the bulk temperature is employed:

$$\frac{1}{\bar{\Omega}} \int_{\text{cross section}} \phi \Omega \eta \, d\eta \, d\theta = 1 \tag{11}$$

The boundary conditions for Equation 1 are the no-slip condition ($\Omega = 0$) at the wall ($\eta = a$), and symmetry conditions ($\partial\Omega/\partial n = 0$) at the other boundaries. An isothermal wall boundary condition ($\phi = 0$) is imposed at $\eta = a$ for Equation 2, whereas, at the other boundaries, the symmetry condition ($\partial\phi/\partial n = 0$) applies. In the above relations, a is given by

$$a = \frac{\pi}{2(4-\pi)} \tag{12}$$

The friction factor $f \equiv 2(-dp/dz)D_h/\rho\bar{w}^2$ is calculated via

$$f = \frac{2}{\bar{\Omega}\mathrm{Re}} \tag{13}$$

It can be shown that the average Nusselt number $\mathrm{Nu} \equiv \bar{h}D_h/k$ is given by

$$\overline{\mathrm{Nu}} = \lambda/4 \tag{14}$$

The local Nusselt number $\mathrm{Nu} \equiv hD_h/k$ is evaluated by

$$\mathrm{Nu} = -\left.\frac{\partial\phi}{\partial\eta}\right|_{\eta=a} \tag{15}$$

As implied by the above equations, cylindrical coordinates were employed. Therefore, the channel wall is a line of constant η, whereas the symmetry line normal to the wall is a line of constant θ. The third boundary of the calculation domain, however, is not parallel to any of the coordinate directions.

Equations 1 and 2 were integrated via the finite-volume technique described by Patankar.[14] A nonuniform 92×92 grid was employed, and the irregularity of the domain was tackled with the technique presented by Patankar.[15]

The experiments

The main features of the experimental apparatus, instrumentation, and procedure are now described. Further details can be found in Dutra.[16] The heat transfer coefficients have been determined experimentally with the aid of the naphthalene sublimation technique. This implies that, instead of heat transfer experiments, only mass transfer experiments were performed, and then the corresponding heat transfer coefficients were calculated assuming the analogy between the heat transfer and mass transfer mechanisms to be valid. A detailed description of this technique is available in Souza Mendes.[17]

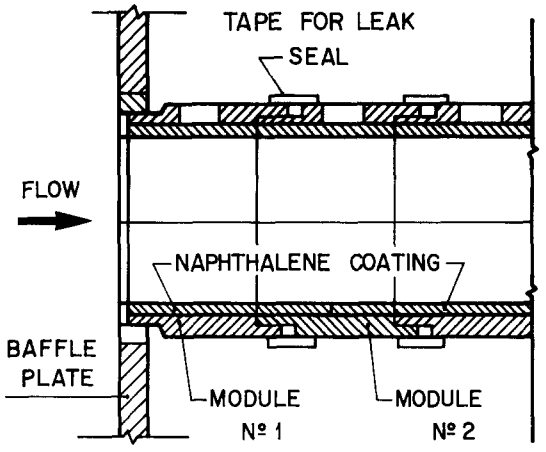

Figure 3 The test section

Test section

The test section was made up of interlocking modules, as illustrated in Figure 3. Each module consisted of a cylindrical metallic (brass) shell whose inner surface was coated with a layer of solid naphthalene. The coating was applied in one module at a time. A four-cusp channel with pure naphthalene walls was obtained when the coated modules were assembled together. Precise mating of successive modules was ensured by interlocking recesses and guiding pins that were provided at the respective ends of each module.

The naphthalene coating procedure is now described. The first step was to remove from all modules, by melting and evaporation, the coating remaining from the preceding data run. Then a mold was assembled. The components of the mold were all made of brass, and included the metallic shell, two end caps, and a shaft with a four-cusp cross section.

The shaft played the role of a centerbody for the casting mold. The surface of the shaft had been polished to a mirrorlike finish. The cavity between the module shell and the shaft was filled with molten naphthalene at $\simeq 190°C$ through a hole drilled across the shell. Once the naphthalene had solidified, the mold was carefully disassembled, and an excellent finish of the resulting naphthalene surface was obtained.

A thermocouple was cast into the naphthalene layer of one of the modules, flush with its inner surface. This module was positioned at the downstream end of the test section, to allow temperature measurements of the naphthalene surface at this axial location.

Air loop

The test section was situated at the upstream end of an open-loop flow circuit that was operated in the suction mode. Air was drawn into the inlet of the test section from the temperature-controlled laboratory room. After leaving the test section, the flowing air entered a flow-metering section (an orifice-plate calibrated meter). Then followed a plenum chamber, a cut-off valve, a control valve, and then a blower. The purpose of the plenum chamber was to dampen oscillations of the air flow induced by the blower. The blower was situated in an adjacent room to avoid thermal and naphthalene contamination.

The test section was oriented horizontally, and its inlet was centered in a large baffle plate. The presence of the baffle created a plenumlike space upstream of the inlet from which the test section drew the air. No smoothing of the edges at the duct entrance was made, i.e., an abrupt inlet condition was employed in the experiments.

Instrumentation

The mass of the naphthalene pieces was measured immediately before and after each data run, to allow the determination of the transport coefficients at each of them. An analytical balance with a resolving power of 0.1 mg and a capacity of 200 g was employed in the mass measurements. Typical changes in mass during a data run were in the range of 0.1 g.

The air flow rate in the test section was determined with an orifice-type flowmeter, fabricated in accordance with the ASME standards and calibrated to ensure its accuracy.

Temperature measurements were made with the aid of two different instruments. The temperature of the naphthalene surface was measured with a thermocouple made of copper-constantan wire. A calibration using a platinum-resistance thermometer indicated a maximum deviation of 0.08°C. The temperature of the air flow approaching the duct inlet was determined with an ASTM 63C mercury thermometer, whose smallest division was 0.1°C. The thermocouple *emf* was read during the course of a data run from a voltmeter having a 1 μV resolution.

Experimental procedure

A few other details about the experimental procedure are now discussed, in addition to the several aspects that have already been mentioned. The naphthalene-coated modules were left in the air-conditioned laboratory room overnight in order to attain thermal equilibrium with the room air. To avoid sublimation and to guarantee an ambient air free from naphthalene vapor in the laboratory, the modules were kept in an air-tight plastic bag during the equilibration period.

Just before the beginning of a data run, the modules were individually weighed and then assembled to form the test section. The blower had been warmed up in advance to provide a steady flow from the moment of activation. After the period of duration of the run, the test section was disassembled and the modules reweighed. During all of these operations, the modules were never touched with bare hands; insulated gloves were used for this purpose.

To obtain a correction for possible extraneous sublimation that might have occurred between the two weighings, a so-called after-run was performed. During the after-run, the whole procedure of the actual data run was repeated, except for the fact that the blower was never activated. The mass measurements following the after-run provided the sought-for correction, which was never larger than 2% of the total mass sublimed per piece.

Data reduction

The per-module mass transfer coefficient, K_i, for the ith module was evaluated from the defining equation

$$K_i = \frac{\dot{M}_i}{A_w} \Delta\rho_{n,i} \tag{16}$$

The mass transfer rate $\dot{M}_i$ is determined by taking the ratio between the (corrected) amount of mass sublimed from module i and the time duration τ of the data run, i.e, $\dot{M}_i = M_i/\tau$.

The difference in naphthalene vapor densities that appears in Equation 16 is the log-mean density difference corresponding to the ith module, defined as

$$\Delta\rho_{n,i} \equiv \frac{(\rho_{nw} - \rho_{nb,i-1}) - (\rho_{nw} - \rho_{nb,i})}{\ln[(\rho_{nw} - \rho_{nb,i-1})/(\rho_{nw} - \rho_{nb,i})]} \tag{17}$$

The quantity ρ_{nw} is the density of naphthalene vapor at the duct wall, and is evaluated with the aid of the perfect-gas law. Therefore, $\rho_{nw} = M_n p_{nw}/\mathscr{R} T_w$, where M_n is the molecular weight of naphthalene vapor, equal to 128.17[19], and $\mathscr{R}$ is the universal perfect-gas constant. The duct wall temperature T_w is measured with the thermocouple embedded in the naphthalene layer. The vapor pressure of naphthalene vapor p_{nw} is evaluated at the wall temperature according to Sogin's[17] expression

$$\ln p_{nw} = 31.23252 - \frac{8587.36}{T_w} \tag{18}$$

The other quantities that appear in Equation 17 are $\rho_{nb,i-1}$ and $\rho_{nb,i}$. They represent, respectively, the bulk vapor density at the inlet and exit of the ith module. Clearly,

$$\rho_{nb,i} = \rho_{nb,i-1} + \frac{\dot{M}_i}{\dot{m}/\rho} \tag{19}$$

where $\dot{m}$ is the air mass flow rate and ρ is the air density, evaluated at the inlet conditions. Assuming that the air at the test section inlet is free from naphthalene vapor, i.e., $\rho_{nb,0} = 0$, then

$$\rho_{nb,i} = \sum_{j=1}^{i} \frac{\dot{M}_j}{\dot{m}/\rho} \tag{20}$$

The dimensionless counterpart of the mass transfer coefficient is the Sherwood number Sh_i, defined as

$$\mathrm{Sh}_i = \frac{K_i D_h}{\nu} \mathrm{Sc} \tag{21}$$

where the Schmidt number Sc is equal to 2.5 for naphthalene diffusion in air. The kinematic viscosity ν was also evaluated at the air inlet conditions.

Numerical results

The results obtained with the numerical solution of the laminar fully developed flow through the four-cusp channel are now presented. The ratio between maximum and mean axial velocities in the channel was found to be

$$\frac{w_{max}}{\bar{w}} = \frac{\Omega_{max}}{\bar{\Omega}} = 2.38 \tag{22}$$

This ratio is larger for the present flow than for the flow in the circular tube. This fact is in accordance with expectations, since the large amount of wetted area in the four-cusp channel yields very low velocities in a large portion of its cross-sectional area.

The friction factor was evaluated numerically via Equation 13, and turned out to be equal to

$$f = \frac{26.3}{\mathrm{Re}} \tag{23}$$

The constant 26.3 in the above equation is much lower than 64, which is the value for the circular tube. This trend is also found in other channels, such as triangular ducts.

Figure 4 shows the distribution of the local Nusselt number along the wall at a given axial location in the fully developed region. A comparison of this figure with the results reported in ref. 13 for another thermal boundary condition reveals that the qualitative behavior is the same, and that for uniform wall temperature (present results) the Nusselt number is lower. It can be seen from this figure that, as the angular coordinate θ increases ($\theta = 0°$ at the cusp), the local Nusselt number increases, and displays a maximum value of 3.59 at $\theta = 45°$. It may also be observed that the portion of wall in the neighborhood of the cusp ($0 < \theta < 15°$) is nearly inactive as far as heat transfer is concerned.

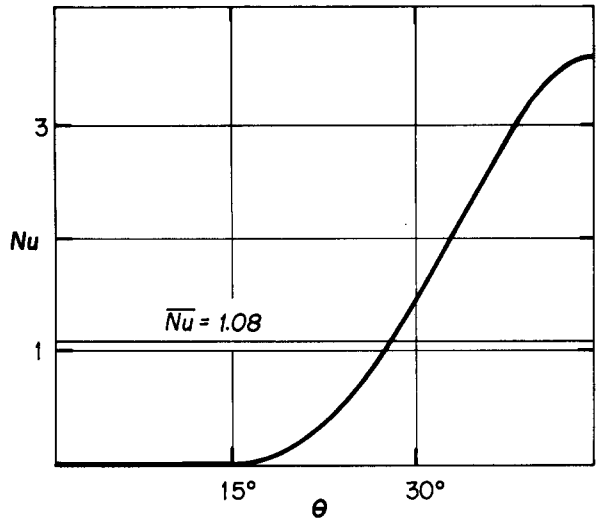

Figure 4 Local Nusselt number for laminar flow

This behavior is easily understood if it is observed that, in the portion of the cross section located close to the cusp, there is almost no flow, due to the narrow passages encountered. Therefore, heat transfer should be very poor at the portion of the wall close to this region. On the other hand, the portion of channel wall which is exposed the most to the flow is exactly the one located the farthest from the cusp, i.e., at $\theta = 45°$. Therefore, it is reasonable to find the highest heat transfer rate at this location.

The mean Nusselt number at a given axial location in the fully developed portion of the flow was found to be equal to

$$\overline{Nu} = 1.08 \tag{24}$$

for laminar flow. This result agrees well with refs. 11 and 12. It is worth noting that the average Nusselt number predicted by the simple relation given in Figure 3.7 of ref. 18 is equal to 1.00 for this geometry.

Comparing this result with the result for the circular tube, namely, $\overline{Nu} = 3.66$, it can be concluded that the heat transfer performance of the four-cusp channel in laminar flow is dramatically poor. This low mean value is clearly due to the nearly inactive portion of the heat transfer area in the vicinity of the cusp.

Experimental results

The transport coefficients presented in this section have been obtained from mass transfer experiments. Therefore, they appear in the form of dimensionless mass transfer coefficients, i.e., Sherwood numbers. Since naphthalene sublimation was employed, the data pertain to a Schmidt number $Sc = 2.5$. However, as mentioned earlier, the analogy between heat and mass transfer implies that all Sherwood numbers obtained for $Sc = 2.5$ are also Nusselt numbers Nu for Prandtl number $Pr = 2.5$ (and for a boundary condition of uniform wall temperature). Because of this, the phrases *heat transfer* and *mass transfer* will be used interchangeably in the presentation of the experimental results.

Entrance region results

The axial distribution of the Sherwood number is given in Figure 5 for some representative values of the Reynolds number. The data for each value of the Reynolds number are identified by a different symbol. In this figure, the per-module Sherwood number is plotted as a function of the dimensionless axial coordinate z/D_h, which has its origin at the duct inlet and increases in the flow direction. The per-cycle average Sherwood number of each module is plotted in these figures at the axial position corresponding to the module's midpoint.

From this figure, it is seen that the entrance region is rather short in the four-cusp channel. The flow becomes fully developed after about five hydraulic diameters for $Re = 5300$, after about seven hydraulic diameters for $Re = 14{,}800$, and after about eight hydraulic diameters for $Re = 30{,}300$. Qualitatively, the trends shown in Figure 5 are also found in many other flows through channels whose cross sections do not vary along their lengths.

It may be observed that a larger number of modules in the entrance region would be desirable for some of the cases investigated, to yield a better resolution for the *local* information. However, this was not possible due to practical limitations.

Fully developed results

As observed in Figure 5, the Sherwood number Sh tends to an asymptotic value in the region far from the channel inlet. These fully developed values of Sh are plotted in Figure 6 as a function of the Reynolds number. The figure suggests that this fully developed value of the per-module Sherwood number Sh_{fd} has a dependence on the Reynolds number of the power-law type. A least-squares fit to these data yields

$$Sh_{fd} = 0.0645 Re^{0.672} \tag{25}$$

The well-known Dittus–Boelter equation is also plotted (for $Pr = Sc = 2.5$) in Figure 6. A comparison between the two curves readily yields that the four-cusp channel displays a much poorer performance as far as heat transfer is concerned. This behavior agrees with the expectations, since a large portion of the heat transfer area is in the neighborhood of a cusp, where very low fluid velocities prevail.

It is interesting to consider now the ratio $\overline{Nu}/\overline{Nu}_{ct}$ between the Nusselt number for the four-cusp channel and the Nusselt number for the circular tube. For laminar flow, $\overline{Nu}/\overline{Nu}_{ct} = 1.08/3.66 = 0.29$. For turbulent flow, if Equation 25 is employed in conjunction with the Dittus–Boelter equation, $\overline{Nu}/\overline{Nu}_{ct} = 1.9435 Re^{-0.128}$, varying between 0.51 and 0.6 in the range of

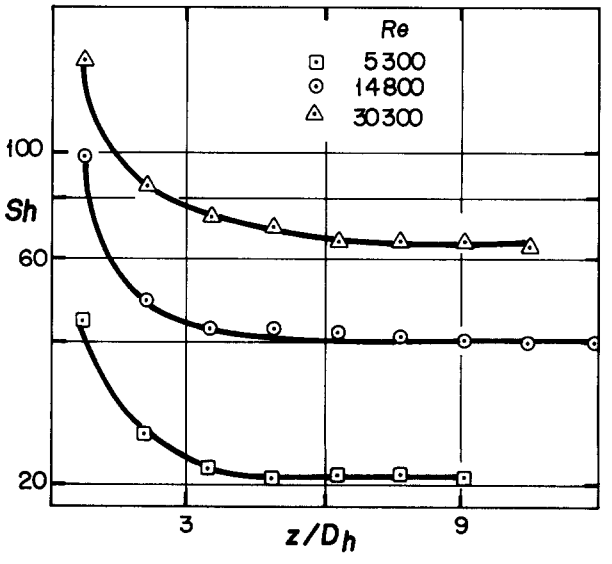

Figure 5 Effect of Reynolds number on axial distributions of the Sherwood number

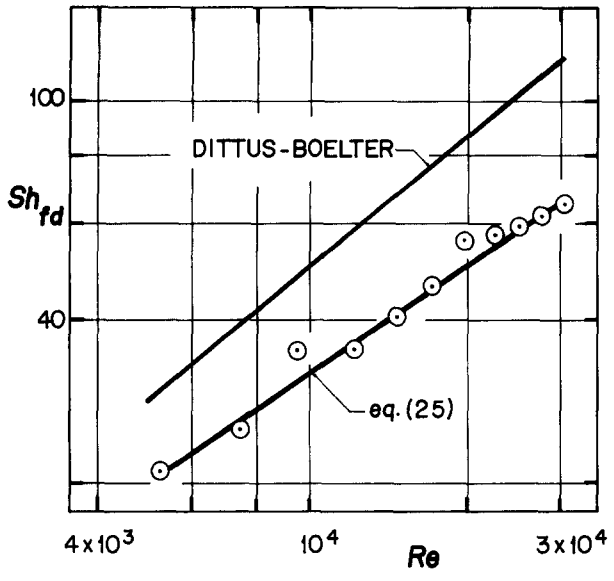

Figure 6 Effect of Reynolds number on the fully developed Sherwood number

Re investigated. Therefore, the heat transfer performance of the four-cusp channel is clearly worse for laminar flow.

If the dependence of the Nusselt number $\overline{Nu}$ on the Prandtl number Pr is assumed to be of the power-law type[17] with an exponent equal to 0.4, then Equation 25 may be used for heat transfer to fluids with Prandtl numbers other than 2.5. In this case, it may be written that

$$\overline{Nu} = 0.0447 Pr^{0.4} Re^{0.672} \quad (26)$$

Conclusions

The research described here constitutes a study of the heat transfer characteristics of the laminar and turbulent flow in a four-cusp channel with uniform wall temperature. For laminar flow, a numerical solution was obtained, whereas an experimental analysis was performed for turbulent flow. In the experiments, the Reynolds number was varied in the range $5300 < Re < 30{,}300$.

The results obtained with the numerical solution of the laminar fully developed flow showed that the ratio between maximum and mean axial velocities in the channel is equal to 2.38, being larger than for the flow in the circular tube. This is due to the large amount of wetted area in the four-cusp channel, which yields very low velocities in a large portion of its cross-sectional area.

The product fRe for the four-cusp channel was found to be equal to 26.3, which is lower than for flow in a circular tube.

The local Nusselt number is negligibly small in the cusp region ($0 < \theta < 15°$), and increases with the θ-coordinate up to a maximum value of 3.59 at $\theta = 45°$. The mean Nusselt number is equal to 1.08, which is much lower than the corresponding value for the circular tube, due to the nearly inactive portion of the heat transfer area in the vicinity of the cusp.

For turbulent flow, the experimental results for the axial distribution of the Sherwood number showed that the entrance region of the flow is very short, varying from five to eight hydraulic diameters in the Re range investigated. An abrupt inlet condition was employed in the experiments.

As was also observed for laminar flow, the fully developed Nusselt number for turbulent flow in a four-cusp channel is much lower than the Nusselt number in the circular tube, due to the negligible heat transfer occurring at the portion of the wall in the neighborhood of a cusp.

The ratio between the Nusselt number for the four-cusp channel and the Nusselt number for the circular tube is equal to 0.29 for laminar flow, and varies between 0.51 and 0.6 for turbulent flow, in the range of Re investigated. Therefore, the heat transfer performance of the four-cusp channel is worse for laminar flow.

Finally, it should be emphasized that all results reported in this article pertain to a thermal boundary condition of uniform temperature at the solid wall; on the other hand, under LOCA-conditions a nonuniform temperature distribution at the cladding occurs. It is well known that, for laminar internal flows, the Nusselt number depends significantly on the thermal boundary condition at the wall.

Therefore, care should be taken in any attempt to apply the present results in LOCA simulations with laminar flow conditions. For turbulent internal flows, however, the heat transfer rate at the wall is much less dependent on the thermal boundary condition, and this dependence decreases as the Reynolds number is increased.

References

1 Rose, K., Mann, C. A., and Hindle, E. D. The axial distribution of deformation in the cladding of pressurized water reactor fuel rods in a loss-of-coolant accident. *Nucl. Technol.*, 1979, **46**, 220–227

2 Turner, J. T. and Haque, M. A. Pressurized water reactor blockage: an experimental study of fluid flow and heat transfer in a model core. *Inst. Mech. Engineers*, 1983, **C106/83**, 163–173

3 Kawasaki, S., Hashimoto, H., Otomo, T., Furuta, T., and Uetsuka, H. The effect of burst temperature on coolant channel restriction in multirods burst tests. *J. Nucl. Sci. Technol.*, 1983, **20**(3), 246–253

4 Gunn, D. J. and Darling, C. W. W. Fluid flow and energy losses in non-circular conduits. *Trans. Inst. Chem. Engineers*, 1963, **41**, 163–173

5 Gerard, R. and Baines, W. D. Turbulent flow in very noncircular conduit. *J. Hyd. Div., ASCE*, 1977, **103**(HY8), 829–841

6 Hall, W. B., Ioannou, G. P., and Turner, J. T. Heat transfer in the vicinity of a partial flow blockage in a reactor core. *Proc. Inst. Mech. Engineers, Conf. on Heat Transfer and Fluid Flow in Water Reactor Safety*, 1977, **C212/77**, 143–147

7 Haque, M. A., Hassan, A. K. A., Turner, J. T., and Barrow, H. The prediction of forced convection in a cusp shaped channel, *Proc. 7th Int. Heat Transfer Conf.*, Munich, 1982, **5**, 459–465

8 Hassan, A. K. A. and Barrow, H. A numerical investigation of turbulent flow and conjugate heat transfer in a 4-cusp channel. *UK Natl. Conf. on Heat Transfer*, Leeds, 1984, **1**, 337–346

9 Ihle, P. and Rust, K. Flow blockage effects on reflood heat transfer in 25-rod bundles. *Proc. 7th Int. Heat Transfer Conf.*, Munich, 1982, **5**, 475–479

10 Ihle, P. Degraded core heat transfer. *Conf. on Thermohydraulics of Nuclear Reactors*, 1983, **1**, 49–59

11 Maliska, C. R. and Silva, A. F. C. Local effects of highly nonorthogonal grids in the solution of heat transfer problem in cusped corners. *Proc. 1st Int. Conf. on Num. Grid Generation in Comp. Fluid Dynamics*, West Germany, 1986

12 Nieckele, A. O. Analysis of laminar flow with heat transfer in a four-cusp channel. *Report LNCC/CNPq–Brazil* 1986, **011/86** (in Portuguese)

13 Duck, P. W. and Turner, J. T. Pressurized water reactor blockage—prediction of laminar flow and temperature distributions following a loss of coolant accident. *Int. J. Heat Fluid Flow*, 1987, **8**(2), 149–155

14 Patankar, H. V. *Numerical Heat Transfer and Fluid Flow*, McGraw-Hill, New York, 1980

15 Patankar, S. V. A numerical method for conduction in composite materials, flow in regular geometries, and conjugate heat transfer. *Proc. 6th Int. Heat Transfer Conf.*, Toronto, 1978, **3**, 297–304

16 Dutra, A. S. Transport coefficients in four-cusp ducts simulating the degraded core of a nuclear reactor. M.S. Thesis 1985, Department of Mechanical Engineering, Pontifícia Universidade Católica-RJ, Rio de Janeiro, Brazil (in Portuguese)

17 Souza Mendes, P. R. The naphthalene sublimation technique. *Proc. First World Conference on Experimental Heat Transfer, Fluid Mechanics and Thermodynamics*, 1988, Elsevier, New York, 446–460

18 Bejan, A. *Convection Heat Transfer*, John Wiley & Sons, New York, 1984

19 Sogin, H. H. Sublimation from disks to air streams flowing normal to their surface. *Trans. ASME*, 1958, **80**, 61–71